



This is a repository copy of *Mega-evolutionary dynamics of the adaptive radiation of birds*.

White Rose Research Online URL for this paper:

<https://eprints.whiterose.ac.uk/110927/>

Version: Accepted Version

Article:

Cooney, C.R., Bright, J.A., Capp, E.J.R. et al. (6 more authors) (2017) Mega-evolutionary dynamics of the adaptive radiation of birds. *Nature*, 542. pp. 344-347. ISSN 0028-0836

<https://doi.org/10.1038/nature21074>

Reuse

Items deposited in White Rose Research Online are protected by copyright, with all rights reserved unless indicated otherwise. They may be downloaded and/or printed for private study, or other acts as permitted by national copyright laws. The publisher or other rights holders may allow further reproduction and re-use of the full text version. This is indicated by the licence information on the White Rose Research Online record for the item.

Takedown

If you consider content in White Rose Research Online to be in breach of UK law, please notify us by emailing eprints@whiterose.ac.uk including the URL of the record and the reason for the withdrawal request.



eprints@whiterose.ac.uk
<https://eprints.whiterose.ac.uk/>

1 **Mega-evolutionary dynamics of the adaptive radiation of birds**

2
3
4 Christopher R. Cooney^{1§}, Jen A. Bright^{1,2,3§}, Elliot J. R. Capp¹, Angela M. Chira¹, Emma
5 C. Hughes¹, Christopher J. A. Moody¹, Lara O. Nouri¹, Zoë K. Varley¹, Gavin H.
6 Thomas^{1,4,*}.

7
8
9 ¹Department of Animal and Plant Sciences, University of Sheffield, Sheffield, S10 2TN,
10 UK

11 ²School of Geosciences, University of South Florida, Tampa, FL 33620, USA

12 ³Center for Virtualization and Applied Spatial Technologies, University of South Florida,
13 Tampa, FL 33620, USA

14 ⁴Bird Group, Department of Life Sciences, The Natural History Museum, Tring,
15 Hertfordshire, UK

16
17
18 § these authors contributed equally

19 * author for correspondence: gavin.thomas@sheffield.ac.uk

26 The origin and expansion of biological diversity is regulated by both
27 developmental trajectories^{1,2} and limits on available ecological niches³⁻⁷. As
28 lineages diversify an early, often rapid, phase of species and trait proliferation
29 gives way to evolutionary slowdowns as new species pack into ever more
30 densely occupied regions of ecological niche space^{6,8}. Small clades such as
31 Darwin's finches demonstrate that natural selection is the driving force of
32 adaptive radiations, but how microevolutionary processes scale up to shape the
33 expansion of phenotypic diversity over much longer evolutionary timescales is
34 unclear⁹. Here we address this problem on a global scale by analysing a novel
35 crowd-sourced dataset of 3D-scanned bill morphology from >2000 species. We
36 find that bill diversity expanded early in extant avian evolutionary history before
37 transitioning to a phase dominated by morphospace packing. However, this early
38 phenotypic diversification is decoupled from temporal variation in evolutionary
39 rate: rates of bill evolution vary among lineages but are comparatively stable
40 through time. We find that rare but major discontinuities in phenotype emerge
41 from rapid increases in rate along single branches, sometimes leading to
42 depauperate clades with unusual bill morphologies. Despite these jumps
43 between groups, the major axes of within-group bill shape evolution are
44 remarkably consistent across birds. We reveal that macroevolutionary processes
45 underlying global-scale adaptive radiations support Darwinian⁹ and Simpsonian⁴
46 ideas of microevolution within adaptive zones and accelerated evolution between
47 distinct adaptive peaks.

48
49 The role of adaptive radiations as the source of much of the world's biological diversity
50 has been widely emphasised^{10,11}. Studies of small clades have provided insights into
51 the role of natural selection as a diversifying force, but cannot illuminate the processes
52 that shape the diversity and discontinuities of radiations over much longer evolutionary
53 timeframes. Indeed, at large taxonomic scales, the diversification of clades^{11,12} and
54 traits¹³ shows no evidence of the predicted slowdowns in evolutionary rates, despite
55 there being numerous examples in small clades^{3,14-16}. This apparent paradox is
56 potentially resolved by G. G. Simpson's model, in which major jumps to new adaptive
57 zones ("quantum evolution") can occur unpredictably throughout clade history. These
58 jumps give rise to rapid lineage expansion into previously unoccupied niche space as
59 sub-clades continue to radiate within distinct adaptive zones and subzones⁴. Simpson's
60 models introduced the concept of 'mega-evolution'—diversification over large temporal
61 and spatial scales—unifying microevolution with other factors such as ecological
62 opportunity and evolutionary constraints that shape the macroevolutionary trajectories
63 of radiating lineages. However, while phylogenetic studies involving thousands of
64 species have demonstrated heterogeneity in rates of phenotypic evolution^{13,17}, it is
65 unclear whether the processes outlined by Simpson play an important role in large-
66 scale adaptive radiations. This is because previous studies have been unable to
67 specifically assess the macroevolutionary dynamics of ecologically relevant traits. Here
68 we study the evolution of an important ecological trait (bill shape) across an entire Class

69 of organisms (birds) to elucidate the processes shaping the accumulation of phenotypic
70 diversity within a global-scale adaptive radiation.

71
72 Our approach is based around a novel data set describing avian bill shape. The avian
73 bill is closely associated with species' dietary and foraging niches^{16,18,19} and represents
74 a highly-adaptable ecological trait known to play a key role in classic avian adaptive
75 radiations^{16,18,20}. We took 3D scans of museum study skins comprising >2000 species
76 (>97% of extant genera) representing the full range of bill shape diversity. We
77 landmarked bills (Extended Data Fig. 1) using a bespoke crowd-sourcing website,
78 www.markmybird.org, and quantified the bill shape morphospace of extant birds using
79 Procrustes superimposition and Principal Components Analyses (PCA, see Methods).
80 The first eight PC axes explain >99% of the total variation in bill shape (Fig. 1). PC1
81 (58% of overall shape variation) describes the volumetric aspect ratio from elongated
82 (e.g. sword-billed hummingbird, *Ensifera ensifera*) to stout bills (e.g. large ground finch,
83 *Geospiza magnirostris*) and captures the range of shape variation encompassed by
84 standard linear measurements (length, width and depth). Variation in these bill
85 dimensions may relate to fine scale division of the dietary or foraging niche among
86 closely related species, but cannot explain the diversity of shapes observed among
87 extant birds. More complex aspects of shape (42% of total variation) are explained by
88 the remaining PCs (Fig. 1), which retain high phylogenetic signal (Extended Data Table
89 1). Importantly, although these higher shape axes explain a low proportion of shape
90 variance, they capture large differences in ecologically relevant aspects of bill shape.
91 The narrow (long tail) distributions of higher shape axes, compared to the broad
92 distribution of PC1 (Extended Data Fig. 2, Extended Data Table 1), suggest that the
93 majority of species have relatively simple bill shapes and diversify in densely packed
94 regions of bill morphospace.

95
96 We tested an important prediction of Simpson's model by evaluating how niche
97 expansion and niche packing have contributed to the accumulation of bill shape
98 disparity throughout avian evolutionary history. We estimated multivariate disparity
99 through time using ancestral state estimates derived from rate heterogeneous models of
100 trait evolution (see Methods)¹³. In 1 million year time slices, we calculated disparity as
101 the sum of the variances²¹ from the first eight shape axes. We compared observed
102 disparity through time with two null models—constant-rate (Brownian motion) and rate
103 heterogeneous trait evolution—that are unbiased with respect to niche filling processes
104 (see Methods). Relative to these null expectations, we find that the filling of avian bill
105 morphospace through time shows a striking dominance of niche expansion early in
106 avian history, followed by a more recent transition towards niche packing (Fig. 2a-b,
107 Extended Data Fig. 2). Our data includes only extant taxa due to the poor preservation
108 of bills in the avian fossil record²², although we acknowledge that some extinct taxa had
109 bills that may lie outside the range of extant diversity (e.g. Phorusrhacidae,
110 Gastornithidae, Dromornithidae). This can result in underestimates of disparity
111 particularly if these morphologies arise early in clade history²²⁻²⁴. Our analyses are
112 therefore conservative with respect to transitions from bill morphospace expansion to

113 filling and consistent with recent studies of avian skeletal material²². The transition in the
114 mode of niche filling is consistent with a process of ever-finer divisions of niche space
115 and would be expected to correspond to slowdowns in rates of bill evolution. However,
116 the switch from niche expansion to niche packing does not map onto temporal trends in
117 the rate of bill shape evolution. Plotting evolutionary rates through time reveals an initial
118 low rate followed by a moderate (two to four-fold) increase that is coincident with the
119 divergence of many non-Passerine orders (Fig. 2c, Extended Data Fig. 3, 4). Thereafter
120 average rates dip and then rise gradually with less than 1.5-fold total variation over ~80
121 million years of evolutionary history, contrasting sharply with >250-fold variation in
122 evolutionary rate among individual lineages (Fig. 3).

123
124 The disjunction between rates of evolution and the accumulation of bill shape disparity
125 suggests that temporal trends in evolutionary rate are not necessarily indicative of the
126 underlying mode of niche filling. This decoupling could arise if some clades diverge
127 rapidly within regions of morphospace that are occupied by other clades, but where the
128 respective clades occur in allopatry. To test this idea, we mapped rates of bill evolution
129 onto the avian phylogeny (Fig. 3, Extended Data Fig. 3-5). We find several instances of
130 clades exhibiting exceptionally high rates of evolution consistent with speciation or
131 phyletic evolution within adaptive subzones (Fig. 3). Some of the fastest rates of bill
132 evolution arise in island radiations of passerine birds, where ecological divergence has
133 been closely linked to ecological opportunity (e.g. Malagasy vangas¹⁶, Galapagos
134 finches¹⁸, Hawaiian honeycreepers²⁰), suggesting that lineages radiating on isolated
135 island archipelagos can explore morphological space independently of the global
136 avifauna. Notably high rates of bill evolution occur in several large species-rich clades
137 that have high speciation rates, including the Psittaciformes, the Furnariidae, and the
138 Passeroidea. However, these clades occupy regions of morphospace that overlap with
139 other more slowly evolving clades and so, while rapid divergence among close relatives
140 within a subzone leads to locally high rates, they do not contribute uniquely to the global
141 expansion of morphospace. In contrast, some large (Anseriformes) and some smaller
142 clades (Alcidae, Bucerotiformes) that exploit more unusual ecological resources have
143 also evolved rapidly.

144
145 Next, we find evidence for several notable instances of exceptionally high rates of
146 evolution along single branches (Extended Data Table 2). Such instances indicate
147 unusually large jumps in bill phenotype and many of the most extreme shifts (e.g.
148 Phoenicopteridae, Musophagidae, Pelecanidae, and Caprimulgiformes; Fig. 3) occur
149 towards the base of the avian radiation, consistent with the idea of early, rapid quantum
150 evolution into new adaptive zones. In some cases (e.g. Pelecanidae and Ciconiidae),
151 the evolution of extreme bill shapes is associated with a subsequent slowdown in the
152 rate of bill shape evolution (Fig. 3), suggesting that ancestral shifts towards a highly
153 specialised bill phenotype may often constrain further opportunities for either bill
154 evolution or speciation²⁵. In contrast, some rapid jumps result in speciose clades
155 occupying more densely packed regions of morphospace. For instance, the
156 Hirundinidae diverge from other Sylvoidea but converge on a swift-like aerial insect

157 hawking form. These latter types of shift do not appear to be restricted to any particular
158 time periods or regions of the avian phylogeny. Similarly, the Trochiliformes diverge
159 rapidly away from the Apodiformes towards a range of bill phenotypes that opened up
160 additional opportunities for continued diversification, consistent with the idea of rapid
161 speciation driven by ecological opportunity following the invasion of an unoccupied
162 adaptive zone^{4,8}.

163
164 Major phenotypic shifts early in the avian adaptive radiation followed by limited
165 divergence within sub-clades, implies a disconnect between mega-evolutionary
166 radiations on a global scale and adaptive radiations within smaller constituent clades.
167 Although the average phenotypes (morphospace centroids) of some higher taxa diverge
168 from one another (Extended Data Fig. 6, 7), it is unclear whether the primary axes of bill
169 shape variation within sub-clades parallel the major axes of variation across birds as a
170 whole (i.e. higher PCs), or whether evolution within clades occurs along axes of
171 variation that are distinct from the major global axes (i.e. lower PCs). We explored these
172 ideas by quantifying the variances and covariances (termed **P** matrices, see Methods)
173 of bill shape axes within higher taxa (families, superfamilies and orders)^{26,27}. We find
174 that shape variation within higher taxa is explained by a single significant eigenvector of
175 **P**, with the exception of the Psittaciformes (two significant eigenvectors). In contrast, the
176 number of significant eigenvectors across all birds combined is three, suggesting that
177 there is low dimensional divergence within clades but high dimensional divergence
178 between clades. We then asked whether the dominant eigenvector within each sub-
179 clade (P_{max}) was consistent across higher taxa. We find that bill shape (i.e. PC) axes 1
180 and 2—those that explain the majority of variation across birds as a whole—also
181 consistently load most heavily onto P_{max} within higher taxa (Extended Data Fig. 7). This
182 suggests that bill shape evolution within higher taxa tends to fall back to limited
183 pathways irrespective of the position of the clade in morphospace

184
185 The low dimensionality and consistency of bill shape variation within clades, and high
186 dimensionality among clades, demonstrates striking discontinuities between how
187 phenotypic disparity accumulates in the early stages of major radiations, versus how
188 disparity accumulates as younger clades evolve within an already mature and
189 ecologically diverse radiation. This early expansion of morphospace has parallels with
190 observations of peak disparity early in clade history in palaeontological datasets of a
191 wide range of metazoan taxa²⁸. The earliest known fossil assemblages of the ancestors
192 of modern birds, dating from the Early Cretaceous, were functionally and ecologically
193 depauperate²⁹. It is likely that the rise of modern birds from the late Cretaceous onwards
194 occurred in a rapidly changing world³⁰, coinciding with extensive ecological opportunity.
195 Our results imply that this dynamic adaptive landscape may have driven Simpsonian
196 mega-evolution across adaptive zones, later giving way to smaller scale fine-tuning of
197 the bill as avian diversity expanded across the globe.

198
199

200 **Methods**

201

202 **Data sampling.** We measured 2,028 species, representing 2,028 of 2,091 genera
203 across 194 families. Specimens were obtained primarily from the avian skin collection at
204 the Natural History Museum, Tring, and also from the Manchester Museum. Study
205 skins, rather than skeletal material, were used because they are generally much better
206 represented in museum collections with more species and specimens available than in
207 skeletons, and secondly because the rhamphotheca (the keratinous sheath surrounding
208 the fused premaxilla, maxilla and nasal bones) is often absent from skeletonised
209 specimens. This is the portion of the bill that interacts directly with the environment and
210 is thus the subject of selection. Where available, one mature male per species was
211 selected for scanning. This was necessary to achieve the taxonomic sampling required
212 within a reasonable time frame and because males are generally better represented in
213 the collections than females. Care was taken to select specimens that were
214 undamaged, with all the landmarks visible and unobstructed (see below). When
215 undamaged males were unavailable, females were preferentially chosen over unsexed
216 specimens. Some species (e.g. Strigiformes, Podargidae, and others) have bills that are
217 obscured by protruding feathers or rictal bristles that ‘shade’ the bill from the scanner.
218 For specimens where this was an issue, or for specimens that were not represented in
219 the skins collections, specimens were chosen from the skeletons collection at Tring.

220

221 **3D scanning and processing.** 3D scans of the bills were taken using white or blue
222 structured light scanning (*FlexScan3D*, LMI Technologies, Vancouver, Canada). The
223 use of 3D scans provides a more complete and nuanced estimate of bill diversity than
224 standard linear measures (length, width, depth) that reflect only the relative proportions
225 of the bill and effectively assume that bills are no more than proportional variations on a
226 cone shape. For bills of lengths > 5 cm, a R3X white-light scanner (calibration boards 10
227 – 25 mm, resolution 0.075 mm) was used, and for bills of lengths < 3 cm a MechScan
228 white-light macro scanner (calibration boards 1.3 – 4 mm, resolution 0.010 mm) was
229 used. For bills intermediate between these lengths, a pre-calibrated HDI blue-light
230 scanner (resolution 0.080 mm) was used. In some cases, larger bills (e.g. those with a
231 high aspect ratio, such as hummingbirds) were scanned on the higher resolution
232 scanner. In order to fully capture 3D geometry, approximately 5 - 25 scans per bill were
233 obtained, and aligned and combined in the *FlexScan* software before being exported as
234 *.ply* files. Scans were imported into *Geomagic Studio* (3D Systems, Rock Hill, SC,
235 USA), automatically decimated to approximately 500,000 faces, and cleaned to remove
236 mesh errors (holes, reversed normals, high aspect ratio spikes). In some specimens, it
237 was necessary to remove feathers or scanning artefacts that had obstructed portions of
238 the geometry by manual cleaning of the mesh. Following cleaning, meshes were
239 exported as *.obj* files.

240

241 **Landmark choice.** Landmark-based geometric morphometrics (GM) is a method for
242 analysing variation in geometric shape based on the positions of equivalent homologous
243 points (landmarks) placed on every specimen in the study^{31,32}. While homologous in this

244 context is usually taken to mean developmentally homologous, in practice the key to
245 landmark selection is that the points chosen must be easily identifiable, such that they
246 can be accurately placed and repeatable within and between specimens³². This is
247 difficult to do on the rhamphotheca because, other than the tip of the bill, it lacks any
248 obvious landmarks, especially as the nostrils are not exposed in many bird species. We
249 therefore opted to identify four true landmarks: 1) the tip of the beak; and the posterior
250 margin of the keratinous rhamphotheca, along the 2) midline dorsal profile; 3) left; and
251 4) right tomial edges. Three semilandmark curves joined point 1 to points 2, 3, and 4 to
252 represent the dorsal profile, and the left and right tomial edges respectively (Extended
253 Data Fig. 1).

254
255 **Crowdsourcing.** In order to facilitate landmarking of such a high number of species, a
256 crowdsourcing website, www.markmybird.org, was developed to allow members of the
257 public to participate in the research by placing landmarks on to the bill scans. After
258 registration, volunteers were required to landmark two training bills with easily
259 identifiable (shoebill, *Balaeniceps rex*) and more challenging (brown-chested alethe,
260 *Alethe poliocephala*) landmarks. Instructions were shown to all users for every
261 landmark, with links to more detailed instructions provided. Bills were assigned to users
262 by randomly selecting a bill from the 100 scans most recently uploaded. To account for
263 the fact that different users will always place homologous landmarks in slightly different
264 places³³, each bill was marked by three to four different users.

265
266 **Quality control and landmark averaging.** Custom R scripts were used to check for
267 common mistakes that may not have been caught by real-time error checks (confusing
268 left and right, large asymmetries in landmark position, incorrect order of semilandmarks,
269 and semilandmarks that deviated from the correct curve due to user failure to rotate the
270 bill and assess their landmark placement in three dimensions). If any landmark
271 configuration failed these tests, the data was manually checked and if necessary
272 removed with the bill made re-available for landmarking. Finally, the three/four
273 repetitions for each bill were averaged to find the mean shape between users, and
274 tested to ensure that all users had placed the landmarks within an acceptable range
275 (Procrustes distance < 0.2) of one another. The average bill shapes were then passed
276 forward for geometric morphometric (GM) analysis. Using ANOVA approaches for
277 assessing measurement error in geometric morphometrics³³, we found that repeatability
278 was consistently high among users when comparing among PC axes (see below;
279 Extended Data Table 2).

280
281 **Geometric morphometrics.** All GM analysis was performed in the R package
282 Geomorph³⁴. First, landmark configurations were subjected to a Generalised Procrustes
283 Analysis (GPA) to remove the effects of size and translational and rotational position on
284 the landmark configurations. This is a common first step in GM analyses as it removes
285 all the geometric information from the landmark coordinates that is not related to
286 shape³¹. During alignment, symmetry was enforced so that slight user-introduced
287 differences in the left/right positions of landmarks were removed. Semilandmarks were

288 slid to minimise bending energy³⁵. The Procrustes aligned coordinates were then
289 assessed using PCA to identify the major axes of shape variation within bird bills, which
290 were plotted as morphospaces. PC scores for the first eight axes are available as
291 supplementary material. As morphospaces are projections of multidimensional Kendall's
292 shape space into two-dimensional tangent space, they may be prone to distortions the
293 further one moves from the central coordinates of the morphospace. In other words,
294 extreme bill morphologies plotting at the edges of morphospace have the potential to
295 distort the projection such that Procrustes distances at the edges of a morphospace are
296 not equivalent to those at the centre of a morphospace. To assess the extent to which
297 projected tangent space differed from the underlying Kendall's shape space, the
298 Procrustes aligned coordinates were analysed using tpsSmall 1.30³⁶. We found no
299 evidence of distortion: distance in tangent was very tightly correlated with Procrustes
300 distance (unc centred correlation: 0.999; regression through the origin slope: 0.985; root
301 mean squared error < 0.001). Similarly, Procrustes distances were consistently close to
302 tangent distances (minimum Procrustes D: 0.024, minimum Tangent d: 0.024; mean
303 Procrustes D: 0.194, mean Tangent d: 0.192; maximum Procrustes D: 0.525, maximum
304 Tangent d: 0.501).

305
306 Warps of the associated shape changes with each PC were generated by transforming
307 the landmarks of the bill closest to the average shape (rusty-fronted barwing, *Actinodura*
308 *egertoni*) to landmarks representing the extremes of a given PC when all other PCs = 0,
309 and interpolating the surface in between.

310
311 To assess any possible distortion of PCA by the underlying phylogenetic non-
312 independence among species, we also ran a phylogenetic PCA^{37,38}. As with the
313 standard PCA, the first eight PCs accounted for >99% of total shape variance. We
314 found that the first two pPCs did not correlate with the first two original PCs—pPC1 was
315 more closely correlated with PC2 and pPC2 was more closely correlated with PC1. The
316 remaining PCs and pPCs were closely correlated and retained the same order in terms
317 of the proportion of variance explained. We also re-ran rate variable models on the first
318 eight pPCs (see below). For this analysis we allowed the pPCs to be correlated
319 because a property of pPCA is that the axes are not expected to be orthogonal. The
320 multivariate results are similar regardless of the choice of PCA or pPCA (Extended Data
321 Fig. 3). Recently identified problems inherent with using PCA (or pPCA) that can lead to
322 misidentifying macroevolutionary models are expected to arise when individual PCs are
323 analysed, particularly when the variance explained is distributed fairly evenly across
324 multiple PCs³⁹. Because we use a multivariate approach these problems are minimized.

325
326 **Phylogenetic framework.** We base our analyses on the phylogenetic tree distributions
327 from www.birdtree.org¹¹. For both 'Hackett' and 'Ericson' backbones, we sampled
328 10,000 'stage 2' trees (i.e. those containing all 9,993 species) from www.birdtree.org,
329 which were pruned to generate tree distributions for the 2,028 species in our dataset.
330 We also generated similar tree distributions using 'stage 1' trees from the same source,
331 which contain only the subset of species placed using genetic data. Of the 2028 species

332 in the full dataset, 1,627 (80%) were represented in stage 1 trees. Based on these
333 distributions, we used TreeAnnotator⁴⁰ to generate maximum clade credibility (MCC)
334 trees, setting branch lengths equal to 'Common Ancestor' node heights. In addition, we
335 constructed a composite of the Jetz et al. trees and the genomic backbone tree of Prum
336 et al.⁴¹ (Extended Data Fig. 4) by grafting sub-clades of the Stage 2 Hackett MCC tree
337 onto nodes in the Prum et al. phylogeny at positions where the two trees could be
338 sensibly combined (see Supplementary Material for node matching data and R code to
339 combine the trees). This process resulted in a composite tree combining the genus level
340 resolution afforded by the Jetz et al. tree with the branching topology and age estimates
341 of the Prum et al. backbone, which are notably younger than those in the Jetz et al.
342 trees.

343
344 **Phylogenetic signal.** We calculated the phylogenetic signal of bill shape by estimating
345 Pagel's λ using the R package MOTMOT⁴². λ can vary between 0 and 1, with a value of
346 0 indicating no phylogenetic signal and a value of 1 indicating similar levels of
347 phylogenetic covariance as expected under a BM model.

348
349 **Models of trait evolution.** Univariate variable rates models were estimated using the
350 software BayesTraits (available from <http://www.evolution.rdg.ac.uk/>) using default
351 priors and a single-chain Markov chain Monte Carlo (MCMC) run for at least 1 billion
352 (1,000,000,000) iterations. From each chain we sampled parameters every 100,000
353 iterations and final parameter estimates for each model were based on 5,000 post-burn
354 in samples. Uncorrelated multivariate models were estimated using the same approach.
355 At each iteration in the MCMC chain, the multivariate models fit a single branch length
356 transformation to the tree across all trait (i.e. PC) axes. An uncorrelated multivariate
357 model is justified because PC axes are inherently orthogonal, however this may limit
358 inference of some forms of rate change. Specifically, the uncorrelated multivariate
359 model is informative with respect to changes in the variances among clades and shifts
360 in the morphospace centroids of clades (i.e. single branch shifts) but cannot detect
361 cases where variances and centroids are similar but covariances among clades differ.
362 We summarised the results of each run by calculating (i) the mean rate and (ii) the
363 probability of a rate shift (branch or clade) over all posterior samples for each node in
364 the tree. It is often challenging to pinpoint the precise location of rate shifts in the tree,
365 particularly when such shifts involve clades of species with short internode intervals at
366 their base. In such cases it becomes difficult to assign the location of a shift to a single
367 node and the inference of a rate shift is then often distributed across two or more nested
368 nodes in the phylogeny. To account for this, we also summarised our results using a
369 second approach in which the posterior probability for a particular rate shift was
370 calculated as the sum of the probability of a shift having occurred on a focal node or on
371 either of the nodes immediately descending from it. We focus on the multivariate
372 analyses because bill shape is a high dimensional trait. In the main text (Fig. 2, 3) we
373 report results from the stage 2 Hackett tree but found comparable results regardless of
374 tree choice (Extended Data Fig. 3, 4).

375

376 We checked for biases in rate estimates across the phylogeny by comparing our
377 observed multivariate rate estimates of bill shape evolution to results generated using
378 simulated data. Using the stage 2 Hackett MCC tree, we generated 10 null multivariate
379 data sets (simulated under BM) and estimated rates using runs of 200 million iterations
380 and 1,000 post-burn samples. We found that on average branch-specific rates derived
381 from simulated data sets were uncorrelated with observed rates of bill shape evolution
382 (Spearman's $\rho = 0.03$; $p = 0.34$), indicating that our results are unlikely to be affected
383 by underlying biases in rate estimation.

384
385 In addition to BayesTraits we compared the fit of three single process models (Brownian
386 motion [BM], early burst [EB] and Ornstein-Uhlenbeck [OU]), fit using the 'fitContinuous'
387 function and default settings in the R package Geiger v2.0⁴³, as well as alternative
388 formulations of the BAMM model⁴⁴ that differed in their handling of temporal rate
389 variation (time constant [T constant], time variable [T var] and time flip [T flip]). The
390 BayesTraits, BAMM and single process models are not fitted in common a framework
391 with consistent likelihood calculations. We therefore compared the fit of the alternative
392 models within each shape axis by calculating the likelihood of a BM model fit to the
393 mean rate-transformed Jetz et al. trees derived from each model. In the absence of
394 support for alternative models (Extended Data Table 3), and because BAMM does not
395 currently allow analyses of multivariate data, we focus our interpretation on analyses
396 using BayesTraits.

397
398 **Disparity and rates through time.** *Estimating ancestral disparity.* We estimated
399 ancestral values for each component axis of bill shape variation using a maximum
400 likelihood approach implemented in the R package phytools³⁸. We estimated ancestral
401 states using the mean rate-transformed trees for each component axis to account for
402 unequal rates of evolution across the tree and among shape axes. To generate
403 estimates of ancestral disparity through time, we took time slices at 1 million year
404 intervals starting at the root of the tree. For each time slice we extracted ancestral state
405 estimates for each component axis for the lineages in the phylogeny existing at that
406 particular time point. We then quantified multivariate disparity in trait values by
407 calculating the sum of the variances across all 8 trait axes²¹. Unlike other disparity
408 metrics, the sum of the variances is expected to be independent of richness and
409 sensitive to changes in both expansion and packing of trait space, thus providing an
410 indication of the relative strength of these two patterns¹⁹.

411
412 *Null models of morphospace filling.* We generated two alternative null models of
413 morphospace filling based on BM models of trait evolution to assess whether the
414 observed patterns of bill shape disparity through time were distinct from unbiased
415 patterns of disparity accumulation. In the first we assumed that trait variation
416 accumulates at a constant rate ('CR') that is homogeneous with respect to time and also
417 to a lineage's position in the phylogeny. In the second we relaxed these assumptions of
418 rate constancy and instead simulated traits using the mean rate-transformed trees for
419 each axis, thereby providing a null model of disparity accumulation incorporating

420 variable rates ('VR') of trait evolution. For each model we simulated 500 replicate data
421 sets and used these to calculate two sets of null disparity through time curves using
422 identical approaches to those describe above. Irrespective of whether evolutionary rates
423 are fixed to be constant or allowed to vary, an important feature of both null models is
424 that the underlying balance between morphospace expansion and packing is expected
425 to be effectively equal and constant over time. This is due to the inherently non-
426 directional nature of trait change simulated using the BM model. Consequently, any
427 deviation in the observed rate of disparity accumulation compared to the null rates
428 suggests that one process (either expansion or packing) has dominated over the other.

429
430 *Summarising evolutionary rates through time.* For each 1 million year time slice, we
431 calculated the mean rate of evolution across all branches present at that time point. We
432 repeated this procedure for each tree in the posterior distribution to generate a
433 distribution of average rate estimates in 1 million year intervals.

434
435 **Estimation of phenotypic variance-covariance (**P**) matrices.** We examined the
436 consistency of bill shape evolution within and among avian clades using Bayesian
437 estimates of phenotypic variance-covariance matrices (**P** matrices) of bill shape within
438 higher taxa (families, superfamilies and orders)^{26,27}. First, we estimated the number of
439 independent axes (i.e. eigenvectors of **P**) that are required to adequately explain the
440 total trait variance in **P** in each higher taxon. We then tested whether the dominant
441 eigenvector of bill shape variation (P_{max}) is consistent among clades. P_{max} is the first
442 principal component of **P** and an estimate of the major axis of phenotypic variation. We
443 estimated phenotypic variance-covariance matrices for higher taxa containing ≥ 20
444 sampled species. Posterior distributions of variance-covariance matrices were
445 generated using Bayesian MCMC MANOVA models implemented in the R package
446 MCMCglmm²⁷. We used weak uniform priors and ran each model for 80,000 iterations
447 with a burn-in of 40,000 and sampling that produced 1,000 estimates of the posterior
448 distribution. Based on these distributions we used a set of Bayesian matrix
449 quantification approaches²⁶ to extract information on (i) centroid position, (ii) subspace
450 orientation, (iii) individual trait loadings onto and variance explained by P_{max} , and (iv)
451 number of significant eigenvectors associated with each **P**.

452

453 **Figure legends**

454
455 **Figure 1. Bird bill morphospace density plots.** PC axes 1-8 are shown as pairwise
456 scatterplots, along with warps representing the change in bill shape ($n = 2028$ species)
457 along each axis in dorsal and lateral views. Each axis is labeled with the proportion of
458 variance explained and estimates of phylogenetic signal (Pagel's λ). The colour scale
459 refers to the number of species in 20 bins with minimum and maximum richness of **a**, 1-
460 23 **b**, 1-72 **c**, 1-64, and **d**, 1-98 species, respectively.

461
462 **Figure 2. Morphospace filling through time.** **a**, Accumulation of multivariate disparity
463 through time in 1 million time slices (thick black line: observed data; thin black line: after
464 LOESS smoothing; blue lines: constant rate null model; red lines: variable rate null
465 model). **b**, Comparison of slopes (estimated in 5 million year windows) of the LOESS-
466 smoothed observed data and null models. Differences in slope above and below zero
467 indicate dominance of morphospace expansion versus morphospace packing
468 respectively. Shading indicates 95% confidence intervals. **c**, Mean relative rates of
469 evolution with 95% confidence intervals (grey) through time.

470
471 **Figure 3. Multivariate rates of bill shape evolution.** The avian phylogeny ($n = 2028$
472 species) coloured by estimates of the mean relative multivariate rate of bill shape
473 evolution. Grey triangles show the stem branch of clades with support for whole clade
474 shifts in evolutionary rate. Coloured circles show rate shifts on individual internal
475 branches (colour indicates the rate estimate). The relative size of triangles and circles
476 indicates the posterior probability (PP) of a rate shift. Triangles distinguish shifts on the
477 focal node (filled) and shifts at the focal node or on one of its two daughter nodes
478 (open).

479
480 **Extended Data Figure 1. Positions of landmarks and semilandmarks.** The image
481 shows a 3D scan of a shoebill (*Balaeniceps rex*) bill marked up with four fixed
482 landmarks (numbered red points) and three semi-landmark curves along the dorsal
483 profile (from points 1 to 2) and tomial edges (left from point 1 to 3 and right from point 1
484 to 4). Each curve consists of 25 semi-landmarks (black points).

485
486 **Extended Data Figure 2. Morphospace density through time.** Plots show the filling
487 of avian bill morphospace through time ($n = 2028$ species) for PCs **a**, 1; **b**, 2; **c**, 3; **d**, 4;
488 **e**, 5; **f**, 6; **g**, 7; and **h**, 8. Densities were calculated in 1 million year time slices based on
489 univariate rate heterogeneous models of trait evolution using a stage 2 Hackett MCC
490 tree from www.birdtree.org. The scale runs from low density (blue) to high density (red),
491 indicating the extent of niche packing through time in different regions of bill
492 morphospace. For each axis the frequency distribution of PC scores among species is
493 also shown (grey bars).

494
495 **Extended Data Figure 3. Comparison of multivariate rates of bill shape evolution**
496 **and disparity through time for alternative datasets.** The plot shows estimates of the

497 mean relative multivariate rate of bill shape evolution for four alternative versions of the
498 avian phylogeny and also when using phylogenetic Principal Components (pPCs) (see
499 Methods). Shown below are plots comparing estimates of disparity and rates through
500 time derived from each dataset. For stage 2 trees $n = 2028$ species and for stage 1
501 trees $n = 1627$ species.

502
503 **Extended Data Figure 4. Multivariate rates of bill shape evolution for a composite**
504 **tree based on the Prum et al. backbone.** The avian phylogeny coloured according to
505 estimates of the mean relative multivariate rate of bill shape evolution. Grey triangles
506 show the stem branch of clades with support for whole clade shifts in evolutionary rate.
507 Coloured circles show rate shifts on individual internal branches (colour indicates the
508 rate estimate). The relative size of triangles and circles indicates the posterior
509 probability (PP) of a rate shift. Filled and open triangles distinguish between shifts on
510 the focal node (filled) and shifts that occur either at the focal node or on one of the two
511 immediate daughter nodes (open).

512
513 **Extended Data Figure 5. Phylogenetic mapping of univariate rates of bill shape**
514 **evolution.** The plots shows the avian phylogeny of all taxa included in the study ($n =$
515 2028 species) with branches coloured on a common scale across panels according to
516 estimates of the univariate rate of bill shape evolution. a, PC1, b, PC2, c, PC3, d, PC4,
517 e, PC5, f, PC6, g, PC7, h, PC8.

518
519 **Extended Data Figure 6. Morphospaces of avian higher taxa.** Pairwise scatterplots
520 of PCs 1 and 2, 3 and 4, 5 and 6, and 7 and 8 showing focal higher taxa (non-
521 passerines, purple; passerines, green) against total avian morphospace (grey). Values
522 in parentheses show the number of species sampled.

523
524 **Extended Data Figure 7. Morphological subspaces of the P of avian higher taxa.**
525 The figure shows representations of **P** for avian higher taxa with ≥ 20 species sampled.
526 First column: distribution of species values on each of the first eight raw PCs showing
527 variation in morphospace centroid for each higher taxon. Second column: two-
528 dimensional subspace for each taxon with non-passerine (purple) and passerine (green)
529 subspaces. The x- and y-axes follow the global leading (P_{max}) and secondary
530 eigenvectors. Third column: percentage of total variance explained and individual PC
531 loadings onto each taxon specific P_{max} . Inset: three-dimensional subspace for all non-
532 passerines (purple) and passerines (green). Values in parentheses show the number of
533 species sampled.

534
535
536 **Extended Data Table 1. Variance, repeatability and phylogenetic signal of PC**
537 **axes.** The table shows individual and cumulative variance values, kurtosis values,
538 scores of among user repeatability (R) and repeatability after averaging (R_n), and
539 maximum likelihood estimates and 95% confidence intervals of Pagel's λ for the first

540 eight PC's of bill shape. λ was estimated using two different tree topologies based on
541 the Hackett and Ericson backbone trees taken from www.birdtree.org.

542
543 **Extended Data Table 2. Summary of major single-lineage bill evolutionary rate**
544 **shifts.** Table shows fold-change rate of evolution and posterior probability (PP) for
545 major (PP > 0.7 and fold-increase > 10) ancestral single-lineage shifts in rate of bill
546 shape evolution.

547
548 **Extended Data Table 3. Comparison of trait models.** The table shows delta likelihood
549 values for alternative models of trait evolution within each shape axis and for different
550 tree topologies. Values were generated by calculating the likelihoods of a BM model fit
551 to the mean rate-transformed trees derived from each model.

552

553 1 Bright, J. A., Marugan-Lobon, J., Cobb, S. N. & Rayfield, E. J. The shapes of bird beaks
554 are highly controlled by nondietary factors. *Proc Natl Acad Sci U S A* **113**, 5352-5357,
555 doi:10.1073/pnas.1602683113 (2016).

556 2 Lamichhaney, S. *et al.* Evolution of Darwin's finches and their beaks revealed by
557 genome sequencing. *Nature* **518**, 371-375 (2015).

558 3 Phillimore, A. B. & Price, T. D. Density-dependent cladogenesis in birds. *PLoS Biol* **6**,
559 e71, doi:10.1371/journal.pbio.0060071 (2008).

560 4 Simpson, G. G. *Tempo and mode in evolution*. (Columbia University Press, 1944).

561 5 Ezard, T. H. & Purvis, A. Environmental changes define ecological limits to species
562 richness and reveal the mode of macroevolutionary competition. *Ecol Lett*,
563 doi:10.1111/ele.12626 (2016).

564 6 Price, T. *Speciation in birds*. 1st edn, (Roberts and Co., 2008).

565 7 Price, T. D. *et al.* Niche filling slows the diversification of Himalayan songbirds. *Nature*
566 **509**, 222-225 (2014).

567 8 Losos, J. B. & Mahler., D. L. in *Evolution Since Darwin: The First 150 Years* (eds M. A.
568 Bell, D. J. Futuyma, W. F. Eanes, & J. S. Levinton) 381-420 (Sinauer Associates, 2010).

569 9 Reznick, D. N. & Ricklefs, R. E. Darwin's bridge between microevolution and
570 macroevolution. *Nature* **457**, 837-842, doi:10.1038/nature07894 (2009).

571 10 Alfaro, M. E. *et al.* Nine exceptional radiations plus high turnover explain species
572 diversity in jawed vertebrates. *Proc Natl Acad Sci U S A* **106**, 13410-13414,
573 doi:10.1073/pnas.0811087106 (2009).

574 11 Jetz, W., Thomas, G. H., Joy, J. B., Hartmann, K. & Mooers, A. O. The global diversity of
575 birds in space and time. *Nature* **491**, 444-448, doi:10.1038/nature11631 (2012).

576 12 Hedges, S. B., Marin, J., Suleski, M., Paymer, M. & Kumar, S. Tree of life reveals clock-
577 like speciation and diversification. *Mol Biol Evol* **32**, 835-845,
578 doi:10.1093/molbev/msv037 (2015).

579 13 Venditti, C., Meade, A. & Pagel, M. Multiple routes to mammalian diversity. *Nature* **479**,
580 393-396, doi:10.1038/nature10516 (2011).

581 14 Etienne, R. S. *et al.* Diversity-dependence brings molecular phylogenies closer to
582 agreement with the fossil record. *Proc Biol Sci* **279**, 1300-1309,
583 doi:10.1098/rspb.2011.1439 (2012).

584 15 Rabosky, D. L. & Glor, R. E. Equilibrium speciation dynamics in a model adaptive
585 radiation of island lizards. *P Natl Acad Sci USA* **107**, 22178-22183,
586 doi:10.1073/pnas.1007606107 (2010).

587 16 Jonsson, K. A. *et al.* Ecological and evolutionary determinants for the adaptive radiation
588 of the Madagascan vangas. *Proc Natl Acad Sci U S A* **109**, 6620-6625,
589 doi:10.1073/pnas.1115835109 (2012).

590 17 Rabosky, D. L. *et al.* Rates of speciation and morphological evolution are correlated
591 across the largest vertebrate radiation. *Nat Commun* **4**, 1958, doi:10.1038/ncomms2958
592 (2013).

593 18 Grant, P. R. *Ecology and evolution of Darwin's finches*. 2nd edn, (Princeton University
594 Press, 1999).

595 19 Pigot, A. L., Trisos, C. H. & Tobias, J. A. Functional traits reveal the expansion and
596 packing of ecological niche space underlying an elevational diversity gradient in
597 passerine birds. *Proc Biol Sci* **283**, doi:10.1098/rspb.2015.2013 (2016).

598 20 Lovette, I. J., Bermingham, E. & Ricklefs, R. E. Clade-specific morphological
599 diversification and adaptive radiation in Hawaiian songbirds. *Proc Biol Sci* **269**, 37-42,
600 doi:10.1098/rspb.2001.1789 (2002).

601 21 Kraft, N. J. B., Valencia, R. & Ackerly, D. D. Functional traits and niche-based tree
602 community assembly in an amazonian forest. *Science* **322**, 580-582 (2008).

603 22 Mitchell, J. S. Extant-only comparative methods fail to recover the disparity preserved in
604 the bird fossil record. *Evolution* **69**, 2414-2424 (2015).

605 23 Finarelli, J. A. & Goswami, A. Potential Pitfalls of Reconstructing Deep Time
606 Evolutionary History with Only Extant Data, a Case Study Using the Canidae
607 (Mammalia, Carnivora). *Evolution* **67**, 3678-3685 (2013).

- 608 24 Slater, G. J. Iterative adaptive radiations of fossil canids show no evidence for diversity-
609 dependent trait evolution. *P Natl Acad Sci USA* **112**, 4897-4902 (2015).
- 610 25 Ricklefs, R. E. Small clades at the periphery of passerine morphological space. *Am Nat*
611 **165**, 651-659, doi:10.1086/429676 (2005).
- 612 26 Robinson, M. R. & Beckerman, A. P. Quantifying multivariate plasticity: genetic variation
613 in resource acquisition drives plasticity in resource allocation to components of life
614 history. *Ecol Lett* **16**, 281-290, doi:10.1111/ele.12047 (2013).
- 615 27 Hadfield, J. D. MCMC Methods for Multi-Response Generalized Linear Mixed Models:
616 The MCMCglmm R Package. *J Stat Softw* **33**, 1-22 (2010).
- 617 28 Hughes, M., Gerber, S. & Wills, M. A. Clades reach highest morphological disparity early
618 in their evolution. *Proc Natl Acad Sci U S A* **110**, 13875-13879,
619 doi:10.1073/pnas.1302642110 (2013).
- 620 29 Mitchell, J. S. & Makovicky, P. J. Low ecological disparity in Early Cretaceous birds. *P*
621 *Roy Soc B-Biol Sci* **281** (2014).
- 622 30 Brusatte, S. L., O'Connor, J. K. & Jarvis, E. D. The Origin and Diversification of Birds.
623 *Curr Biol* **25**, R888-898, doi:10.1016/j.cub.2015.08.003 (2015).
- 624 31 Klingenberg, C. P. Visualizations in geometric morphometrics: how to read and how to
625 make graphs showing shape changes. *Hystrix* **24**, 15-24 (2013).
- 626 32 Zelditch, M. *Geometric morphometrics for biologists : a primer*. (Elsevier Academic
627 Press, 2004).
- 628 33 Fruciano, C. Measurement error in geometric morphometrics. *Dev Genes Evol* **226**, 139-
629 158 (2016).
- 630 34 Adams, D. C. & Otarola-Castillo, E. geomorph: an r package for the collection and
631 analysis of geometric morphometric shape data. *Methods Ecol Evol* **4**, 393-399 (2013).
- 632 35 Gunz , P., Mitteroecker, P. & Bookstein, F. L. in *Modern Moprhometrics in Physical*
633 *Anthropology* (ed D. E. Slice) 73-98 (Kluwer Academic/Plenum Publishers, 2004).
- 634 36 tpsSmall, testing amount of shape variation, version 1.30 (Department of Ecology and
635 Evolution, State University of New York at Stony Brook, 2014).
- 636 37 Revell, L. J. Size-Correction and Principal Components for Interspecific Comparative
637 Studies. *Evolution* **63**, 3258-3268 (2009).
- 638 38 Revell, L. J. phytools: an R package for phylogenetic comparative biology (and other
639 things). *Methods Ecol Evol* **3**, 217-223 (2012).
- 640 39 Uyeda, J. C., Caetano, D. S. & Pennell, M. W. Comparative Analysis of Principal
641 Components Can be Misleading. *Systematic Biology* **64**, 677-689 (2015).
- 642 40 Drummond, A. J., Suchard, M. A., Xie, D. & Rambaut, A. Bayesian Phylogenetics with
643 BEAUti and the BEAST 1.7. *Molecular Biology and Evolution* **29**, 1969-1973 (2012).
- 644 41 Prum, R. O. *et al.* A comprehensive phylogeny of birds (Aves) using targeted next-
645 generation DNA sequencing. *Nature* **526**, 569-573, doi:10.1038/nature15697 (2015).
- 646 42 Thomas, G. H. & Freckleton, R. P. MOTMOT: models of trait macroevolution on trees.
647 *Methods Ecol Evol* **3**, 145-151, doi:10.1111/j.2041-210X.2011.00132.x (2012).
- 648 43 Pennell, M. W. *et al.* geiger v2.0: an expanded suite of methods for fitting
649 macroevolutionary models to phylogenetic trees. *Bioinformatics* **30**, 2216-2218,
650 doi:10.1093/bioinformatics/btu181 (2014).
- 651 44 Rabosky, D. L. Automatic Detection of Key Innovations, Rate Shifts, and Diversity-
652 Dependence on Phylogenetic Trees. *Plos One* **9** (2014).

653
654
655
656
657
658

659 **Acknowledgements**

660 We thank Mark Adams, Hein van Grouw, and Robert Prys-Jones from the Bird Group at
661 the NHM, Tring and Henry McGhie at the Manchester Museum for providing access to
662 and expertise in the collections; Shai Meiri of Tel Aviv University for providing a sample
663 of study skins; Simon Stone of MechInnovation Ltd. for providing training and advice on
664 3D scanning; Matthew Groves, Jamie McLaughlin, Mike Pidd of HRI Digital for the
665 construction of www.markmybird.org; Andrew Beckerman for advice on analysing **P**
666 matrices; Emily Rayfield, Alex Pigot, Arne Mooers, and Alex White for providing
667 valuable comments on pre-submission drafts of the manuscript. Finally, we are indebted
668 to the wonderful volunteer citizen scientists at www.markmybird.org for generously
669 giving up their time to help build the database of bird bill shape and contribute to our
670 understanding of avian evolution. This work was funded by the European Research
671 Council (grant number 615709 Project 'ToLERates') and by a Royal Society University
672 Research Fellowship to GHT (UF120016).

673

674 **Author information**

675 These authors contributed equally to this work: Christopher R. Cooney & Jen A. Bright.

676

677 **Affiliations**

678 Department of Animal and Plant Sciences, University of Sheffield, Sheffield, S10 2TN,
679 UK

680 Christopher R. Cooney, Jen A. Bright, Elliot J. R. Capp, Angela M. Chira, Emma C.
681 Hughes, Christopher Moody, Lara O. Nouri, Zoë K. Varley, Gavin H. Thomas

682

683 School of Geosciences, University of South Florida, Tampa, FL 33620, USA

684 Jen A. Bright

685

686 Center for Virtualization and Applied Spatial Technologies, University of South Florida,
687 Tampa, FL 33620, USA

688 Jen A. Bright

689

690 Bird Group, Department of Life Sciences, The Natural History Museum, Tring,
691 Hertfordshire, UK

692 Gavin H. Thomas

693

694 **Contributions**

695 Christopher R. Cooney, Jen A. Bright, and Gavin H. Thomas conceived of the study,
696 designed analytical protocols, analysed the data and wrote the manuscript. All authors
697 collected and processed data and provided editorial input into the manuscript.

698

699 **Competing financial interests.** None.

700

701 **Corresponding author**

702 Correspondence to: Gavin H. Thomas

703

704 **Supplementary Information**

705 Excel file (PC_scores_all_genera.csv): this file contains scores for the first eight non-
706 phylogenetic PC's for all species (n = 2028) in our data.
707
708 Excel file (PrumMerge_CRC.xlsx): this file details the mapping of Jetz et al. clades to
709 the Prum et al. backbone phylogeny. The table shows the nodes used to attach patch
710 clades from the Jetz et al. stage 2 Hackett tree to the Prum et al. backbone phylogeny.
711
712 PrumMerge.zip: this archive contains data files and an R script to combine the
713 backbone (approximately family level) phylogeny of Prum et al. with the species level
714 resolution of the Jetz et al avian phylogeny.
715
716 AvianPhylogenies.zip: this archive contains all alternative genus level phylogenies used
717 in our analyses.
718
719 Raw scan data in obj format and text files containing individual and species-averaged
720 landmarks are available from the Natural History Museum Data Portal here:
721 <http://dx.doi.org/10.5519/0005413>.
722

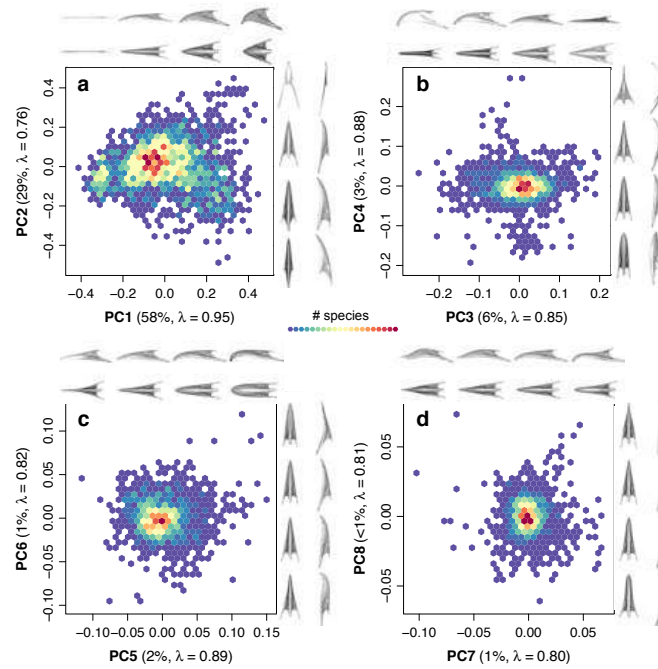


Figure 1. Bird bill morphospace density plots. PC axes 1-8 are shown as pairwise scatterplots, along with warps representing the change in bill shape (n = 2028 species) along each axis in dorsal and lateral views. Each axis is labeled with the proportion of variance explained and estimates of phylogenetic signal (Pagel's λ). The colour scale refers to the number of species in 20 bins with minimum and maximum richness of **a**, 1-23 **b**, 1-72 **c**, 1-64, and **d**, 1-98 species, respectively.

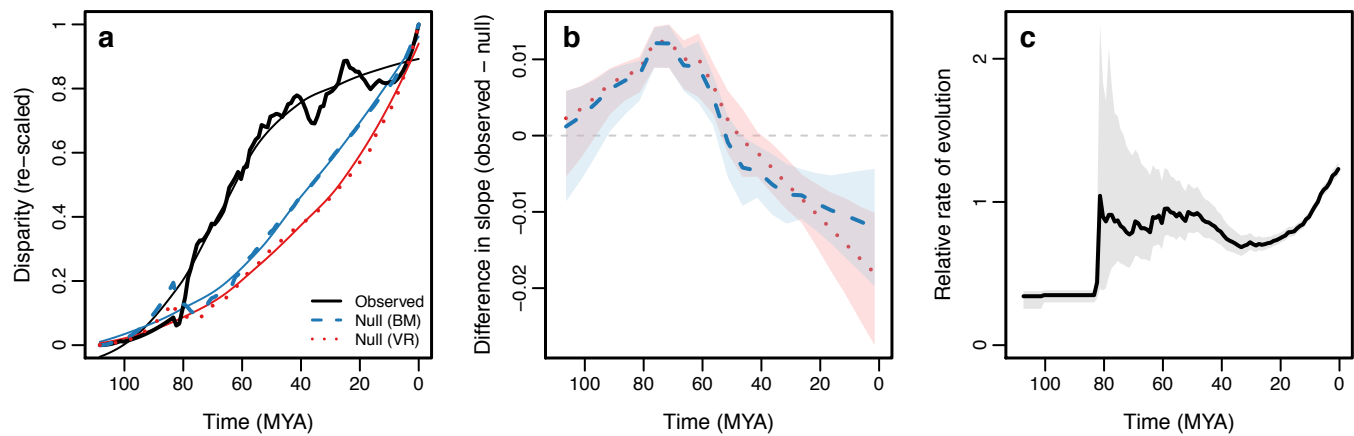


Figure 2. Morphospace filling through time. **a**, Accumulation of multivariate disparity through time in 1 million time slices (thick black line: observed data; thin black line: after LOESS smoothing; blue lines: constant rate null model; red lines: variable rate null model). **b**, Comparison of slopes (estimated in 5 million year windows) of the LOESS-smoothed observed data and null models. Differences in slope above and below zero indicate dominance of morphospace expansion versus morphospace packing respectively. Shading indicates 95% confidence intervals. **c**, Mean relative rates of evolution with 95% confidence intervals (grey) through time.

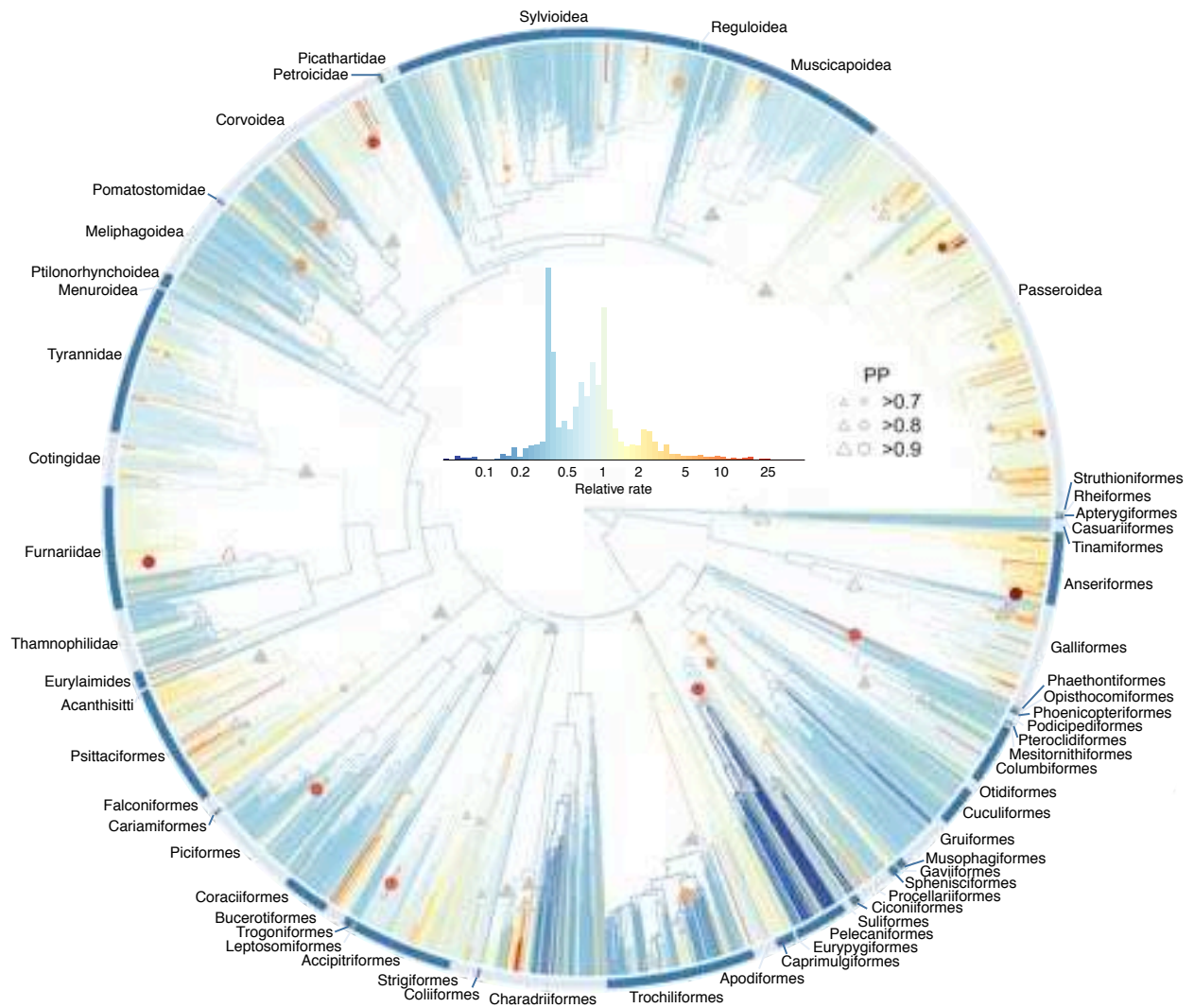
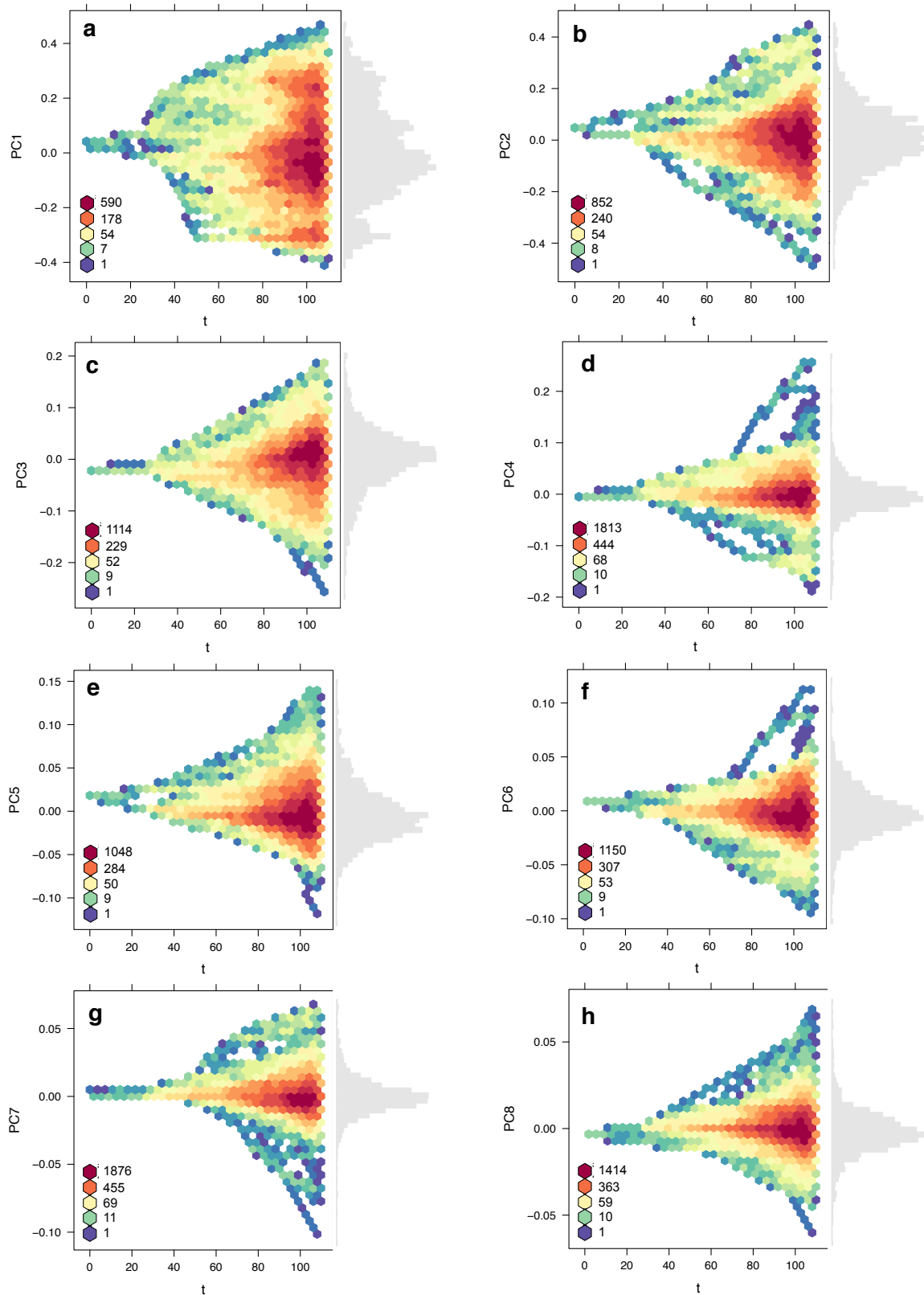


Figure 3. Multivariate rates of bill shape evolution. The avian phylogeny ($n = 2028$ species) coloured by estimates of the mean relative multivariate rate of bill shape evolution. Grey triangles show the stem branch of clades with support for whole clade shifts in evolutionary rate. Coloured circles show rate shifts on individual internal branches (colour indicates the rate estimate). The relative size of triangles and circles indicates the posterior probability (PP) of a rate shift. Triangles distinguish shifts on the focal node (filled) and shifts at the focal node or on one of its two daughter nodes (open).

Extended Data Figures

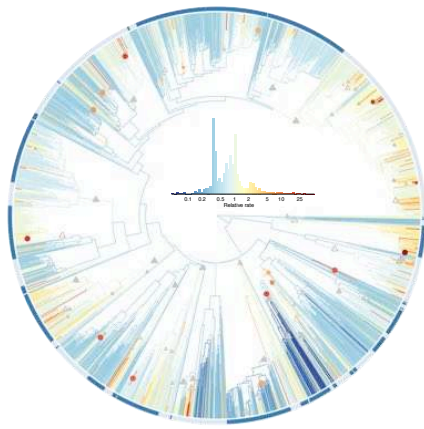


Extended Data Figure 1. Positions of landmarks and semilandmarks. The image shows a 3D scan of a shoebill (*Balaeniceps rex*) bill marked up with four fixed landmarks (numbered red points) and three semi-landmark curves along the dorsal profile (from points 1 to 2) and tomial edges (left from point 1 to 3 and right from point 1 to 4). Each curve consists of 25 semi-landmarks (black points).

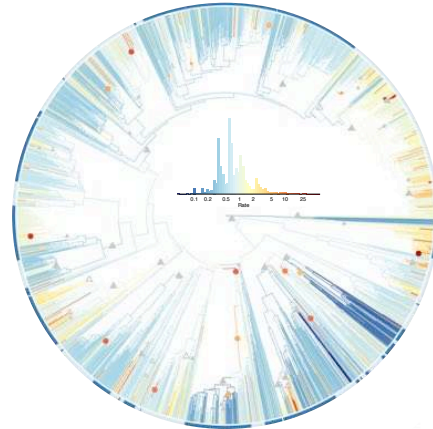


Extended Data Figure 2. Morphospace density through time. Plots show the filling of avian bill morphospace through time ($n = 2028$ species) for PCs **a**, 1; **b**, 2; **c**, 3; **d**, 4; **e**, 5; **f**, 6; **g**, 7; and **h**, 8. Densities were calculated in 1 million year time slices based on univariate rate heterogeneous models of trait evolution using a stage 2 Hackett MCC tree from www.birdtree.org. The scale runs from low density (blue) to high density (red), indicating the extent of niche packing through time in different regions of bill morphospace. For each axis the frequency distribution of PC scores among species is also shown (grey bars).

Stage 2 Hackett

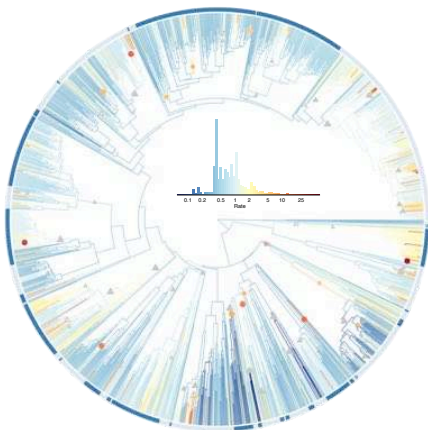


Stage 2 Ericson

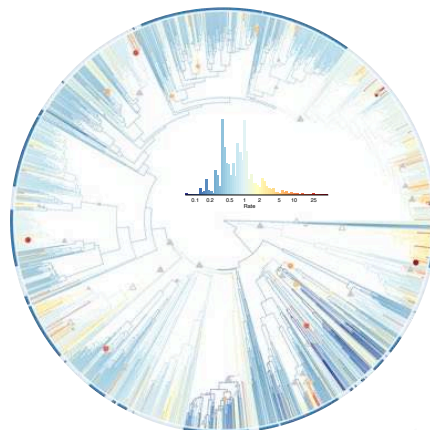


PP PP
 >0.7 >0.7
 >0.8 >0.8
 >0.9 >0.9

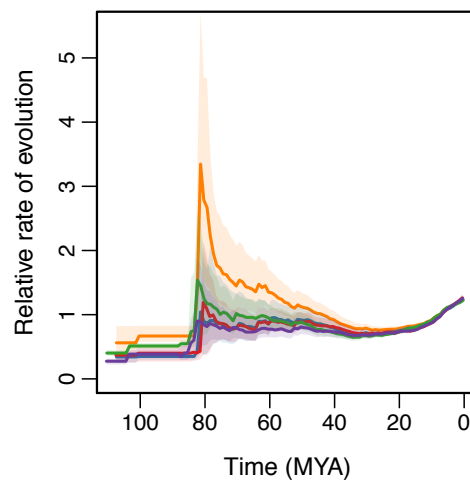
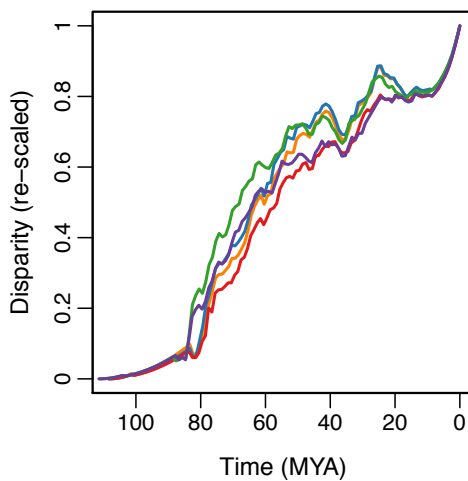
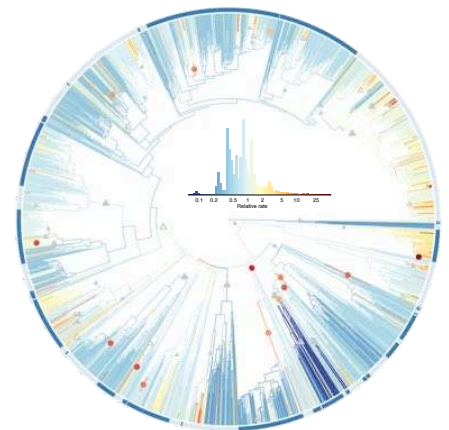
Stage 1 Hackett



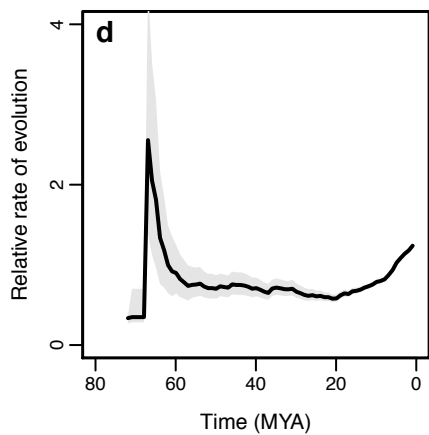
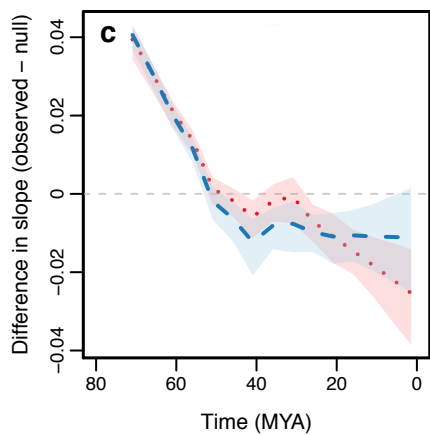
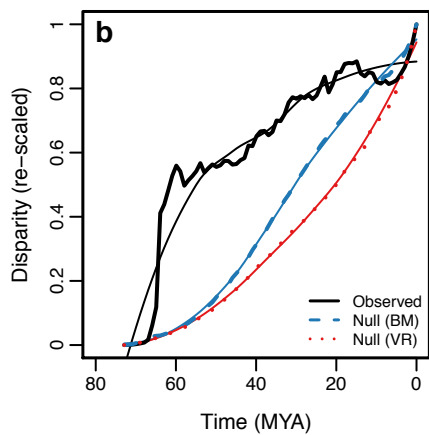
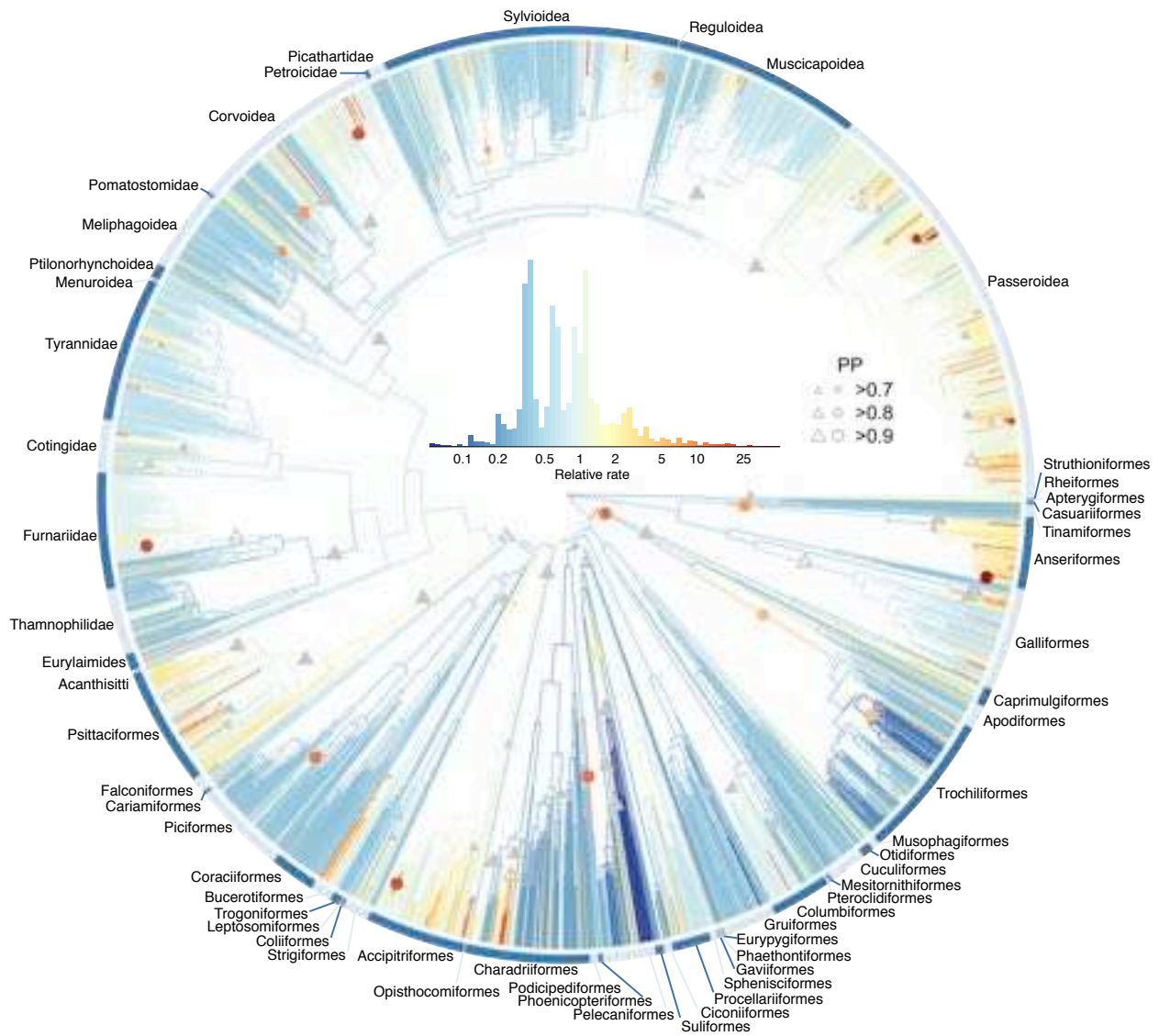
Stage 1 Ericson



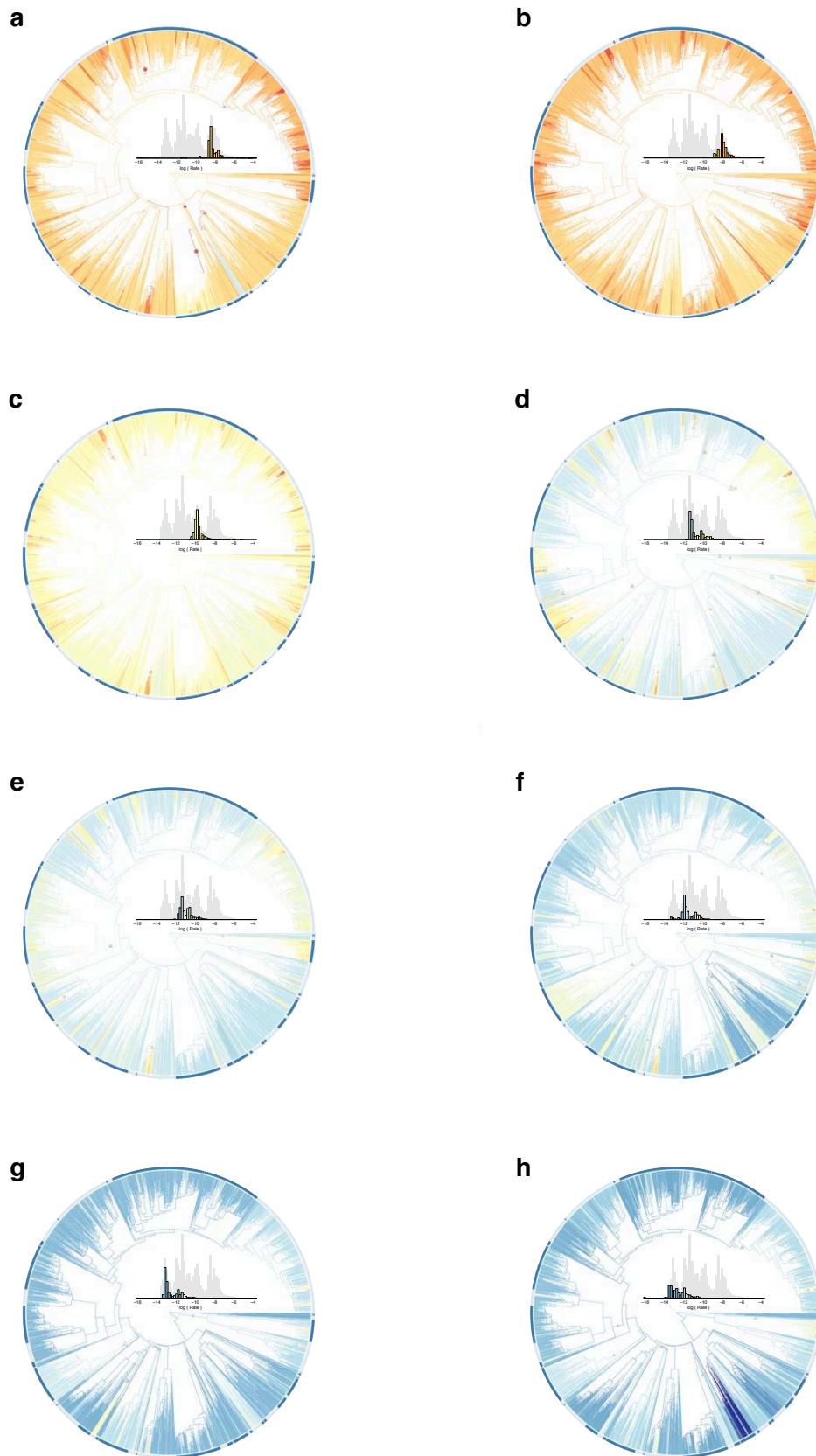
Stage 2 Hackett – pPCs



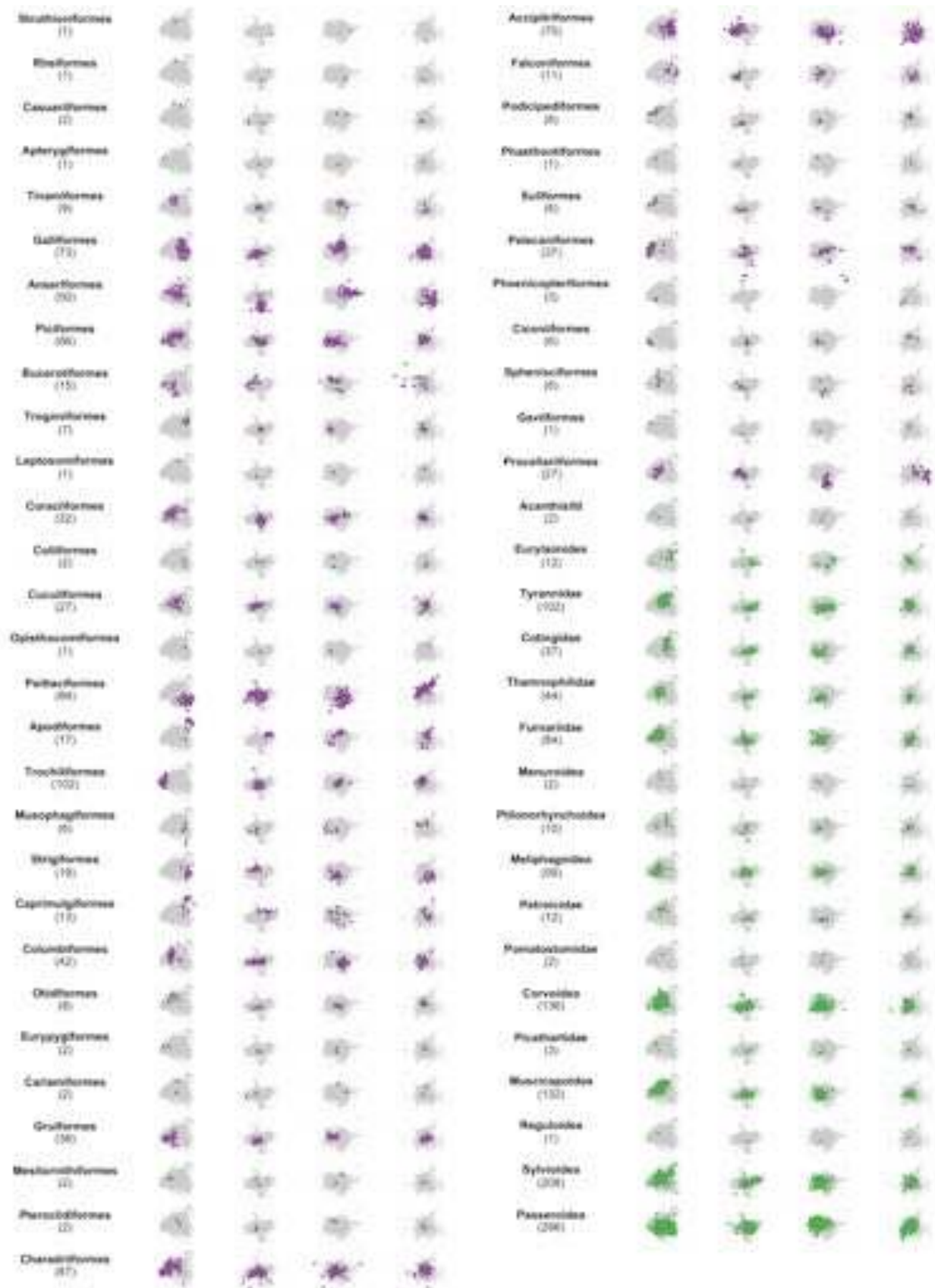
Extended Data Figure 3. Comparison of multivariate rates of bill shape evolution and disparity through time for alternative datasets. The plot shows estimates of the mean relative multivariate rate of bill shape evolution for four alternative versions of the avian phylogeny and also when using phylogenetic Principal Components (pPCs) (see Methods). Shown below are plots comparing estimates of disparity and rates through time derived from each dataset. For stage 2 trees $n = 2028$ species and for stage 1 trees $n = 1627$ species.



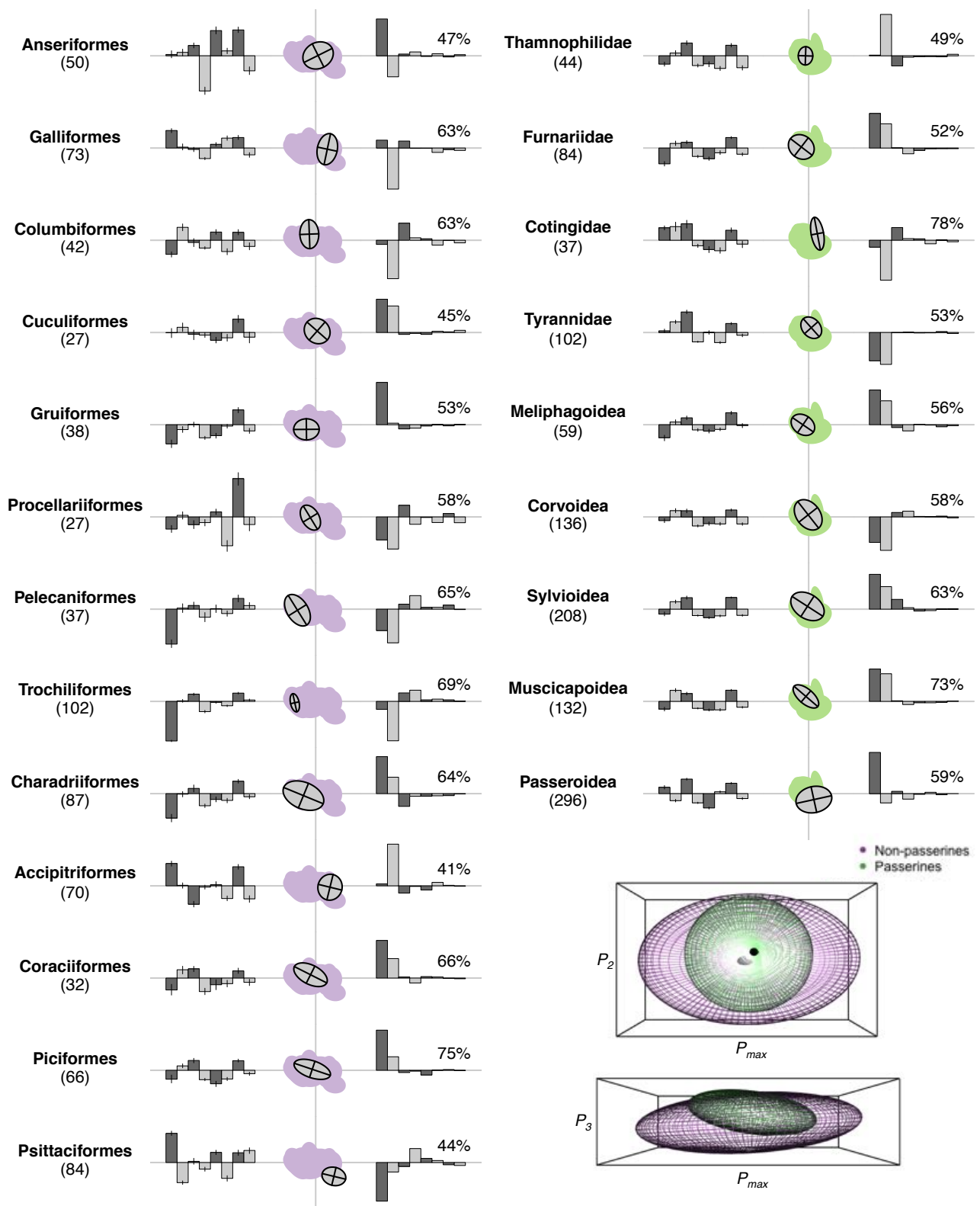
Extended Data Figure 4. Multivariate rates of bill shape evolution for a composite tree based on the Prum et al. backbone. The avian phylogeny coloured according to estimates of the mean relative multivariate rate of bill shape evolution. Grey triangles show the stem branch of clades with support for whole clade shifts in evolutionary rate. Coloured circles show rate shifts on individual internal branches (colour indicates the rate estimate). The relative size of triangles and circles indicates the posterior probability (PP) of a rate shift. Filled and open triangles distinguish between shifts on the focal node (filled) and shifts that occur either at the focal node or on one of the two immediate daughter nodes (open).



Extended Data Figure 5. Phylogenetic mapping of univariate rates of bill shape evolution. The plots shows the avian phylogeny of all taxa included in the study ($n = 2028$ species) with branches coloured on a common scale across panels according to estimates of the univariate rate of bill shape evolution. a, PC1, b, PC2, c, PC3, d, PC4, e, PC5, f, PC6, g, PC7, h, PC8.



Extended Data Figure 6. Morphospaces of avian higher taxa. Pairwise scatterplots of PCs 1 and 2, 3 and 4, 5 and 6, and 7 and 8 showing focal higher taxa (non-passerines, purple; passerines, green) against total avian morphospace (grey). Values in parentheses show the number of species sampled.



Extended Data Figure 7. Morphological subspaces of the P of avian higher taxa. The figure shows representations of P for avian higher taxa with ≥ 20 species sampled. First column: distribution of species values on each of the first eight row PCs showing variation in morphospace centroid for each higher taxon. Second column: two-dimensional subspace for each taxon with non-passerine (purple) and passerine (green) subspaces. The x- and y-axes follow the global leading (P_{max}) and secondary eigenvectors. Third column: percentage of total variance explained and individual PC loadings onto each taxon specific P_{max} . Inset: three-dimensional subspace for all non-passerines (purple) and passerines (green). Values in parentheses show the number of species sampled.

PC axis	Variance (%)	Cumulative (%)	Kurtosis	R	R _n	Stage 2 Hackett λ	Stage 2 Ericson λ
1	57.8	57.8	-0.487	0.998	1.000	0.949 (0.931-0.964)	0.954 (0.936-0.968)
2	29.0	86.8	0.795	0.913	0.976	0.758 (0.704-0.806)	0.760 (0.706-0.808)
3	6.2	93.1	1.381	0.967	0.991	0.851 (0.813-0.882)	0.861 (0.824-0.892)
4	2.8	95.9	7.370	0.987	0.997	0.878 (0.845-0.906)	0.873 (0.838-0.903)
5	1.8	97.7	1.867	0.977	0.994	0.897 (0.863-0.924)	0.888 (0.851-0.917)
6	0.9	98.6	2.122	0.945	0.985	0.822 (0.774-0.863)	0.816 (0.766-0.858)
7	0.4	99.0	6.426	0.953	0.987	0.803 (0.756-0.843)	0.803 (0.756-0.843)
8	0.3	99.2	3.452	0.938	0.983	0.805 (0.752-0.848)	0.794 (0.739-0.840)

Extended Data Table 1. Variance, repeatability and phylogenetic signal of PC axes. The table shows individual and cumulative variance values, kurtosis values, scores of among user repeatability (R) and repeatability after averaging (R_n), and maximum likelihood estimates and 95% confidence intervals of Pagel's λ for the first eight PC's of bill shape. λ was estimated using two different tree topologies based on the Hackett and Ericson backbone trees taken from www.birdtree.org.

Order	Family	Genera	N	Fold-increase	PP
PHOENICOPTERIFORMES	Phoenicopteridae	Phoeniconaias, Phoenicoparrus, Phoenicopterus	3	45.2	1.000
APODIFORMES	Trochilidae	Discosura, Lophornis, Sephanoides	3	38.5	0.999
PELECANIFORMES	Threskiornithidae	Bostrychia, Cercibis, Eudocimus, Geronticus, Lophotibis, Mesembrinibis, Nipponia, Phimosus, Platalea, Plegadis, Pseudibis, Thaumatis, Theristicus, Threskiornis	14	29.6	0.989
PASSERIFORMES	Dendrocolaptidae	Campylorhamphus, Drymornis, Lepidocolaptes	3	23.5	0.994
PASSERIFORMES	Paradisaeidae	Parotia, Pteridophora	2	22.2	0.992
PASSERIFORMES	Melanocharitidae	Oedistoma, Toxorhamphus	2	21.4	0.914
PASSERIFORMES	Platysteiridae	Batis, Platysteira	2	20.1	0.990
PICIFORMES	Ramphastidae	Andigena, Aulacorhynchus, Pteroglossus, Ramphastos, Selenidera	5	18.9	0.988
ANSERIFORMES	Anatidae	Lophodytes, Mergellus, Mergus	3	18.4	0.974
ACCIPITRIFORMES	Accipitridae	Helicolestes, Rostrhamus	2	18.0	0.980
PASSERIFORMES	Hirundinidae	Alochelidon, Atticora, Chamaeocercus, Delichon, Eurochelidon, Haplochelidon, Hirundo, Neochelidon, Notiochelidon, Petrochelidon, Phedina, Progne, Psalidoprocne, Pseudhirundo, Pseudochelidon, Pygochelidon, Riparia, Stelgidopteryx, Tachycineta	19	14.8	0.783
PASSERIFORMES	Fringillidae	Loxioides, Telespiza	2	13.0	0.842
MUSOPHAGIFORMES	Musophagidae	Corythaeola, Corythaixoides, Crinifer, Musophaga, Ruwenzorornis, Tauraco	6	11.5	0.838
PASSERIFORMES	Timaliidae	Jabouilleia, Rimator	2	11.1	0.981

Extended Data Table 2. Summary of major single-lineage bill evolutionary rate shifts. Table shows fold-change rate of evolution and posterior probability (PP) for major (PP > 0.7 and fold-increase > 10) ancestral single-lineage shifts in rate of bill shape evolution.

Tree	PC axis	BayesTraits	BAMM (T var)	BAMM (T flip)	BAMM (T constant)	OU	EB	BM
Stage 2 Hackett	1	0	45.0	171.2	284.5	635.4	630.8	635.4
	2	0	85.3	171.0	280.3	591.4	496.7	591.4
	3	0	48.6	177.1	319.7	595.3	534.0	595.3
	4	0	46.0	156.2	292.2	876.3	830.0	876.3
	5	0	65.1	169.2	294.5	598.9	557.4	598.9
	6	0	41.6	121.8	276.0	703.6	631.8	703.6
	7	0	65.1	170.2	289.3	805.3	718.8	805.3
	8	0	56.4	134.3	281.2	826.8	725.1	826.8
Stage 2 Ericson	1	0	71.3	166.5	302.2	623.6	618.8	623.6
	2	0	82.8	172.5	286.4	575.1	483.4	575.1
	3	0	51.2	164.3	338.7	583.6	529.3	583.6
	4	0	65.5	157.0	283.7	875.0	824.7	875.0
	5	0	59.1	172.6	310.9	625.8	577.1	625.8
	6	0	50.2	128.5	261.3	710.8	636.7	710.8
	7	0	58.6	159.2	297.1	805.7	720.7	805.7
	8	0	69.9	154.1	333.7	831.3	728.2	831.3
Stage 1 Hackett	1	0	56.8	134.7	227.2	479.5	473.6	479.5
	2	0	59.8	149.8	243.1	483.8	398.0	483.8
	3	0	26.4	135.5	271.1	493.5	439.2	493.5
	4	0	40.5	128.4	237.4	714.7	675.2	714.7
	5	0	52.0	136.7	278.4	478.6	439.8	478.6
	6	0	22.6	95.7	219.2	579.5	517.6	579.5
	7	0	26.3	135.1	238.4	670.7	586.1	670.7
	8	0	29.1	103.4	232.2	675.3	570.4	675.2
Stage 1 Ericson	1	0	69.7	132.5	248.7	486.4	479.6	486.4
	2	0	59.4	143.3	239.7	488.2	400.3	488.2
	3	0	21.8	136.4	275.2	502.7	447.2	502.7
	4	0	32.5	132.1	245.3	721.8	679.5	721.8
	5	0	53.8	130.3	275.0	482.9	442.3	482.9
	6	0	23.9	90.3	233.9	583.7	519.5	583.7
	7	0	34.9	132.3	243.6	669.7	585.1	669.7
	8	0	29.5	101.1	244.4	676.4	569.8	676.4

Extended Data Table 3. Comparison of trait models. The table shows delta likelihood values for alternative models of trait evolution within each shape axis and for different tree topologies. Values were generated by calculating the likelihoods of a BM model fit to the mean rate-transformed trees derived from each model.